Dalton Transactions

ROYAL SOCIETY OF CHEMISTRY

PAPER

Check for updates

Cite this: *Dalton Trans.*, 2022, **51**, 9673

Ruthenium-based assemblies incorporating tetrapyridylporphyrin panels: a photosensitizer delivery strategy for the treatment of rheumatoid arthritis by photodynamic therapy†

Manuel Gallardo-Villagrán, [a,b] Lucie Paulus,[b] Jean-Louis Charissoux,[c] David Yannick Leger,[b] Pascale Vergne-Salle,[d] Bruno Therrien *‡[a] and Bertrand Liagre*‡[b]

Received 25th March 2022,
Accepted 29th May 2022

DOI: 10.1039/d2dt00917j

rsc.li/dalton

Ruthenium-based assemblies containing tetrapyridylporphyrins (TPyP) in their structure have been evaluated as photosensitizers (PS) to treat rheumatoid arthritis (RA) by photodynamic therapy (PDT). TPyP is useless by itself as a PS due to its low solubility in biological media, however, incorporated in metallacages it can be internalized in cells. The study shows a cellular antiproliferative activity in fibroblast-like synoviocyte (FLS) in the lower nanomolar range in the presence of light, and no dark toxicity at 1 μM concentration, thus having an excellent photoactivity index. The presence of diamagnetic (Zn^{2+}) and paramagnetic (Co^{2+}) metals in the center of TPyP impairs the effectiveness of PDT, showing no (Co) or reduced (Zn) photoactivity. A total of five metallacages with different structural characteristics have been evaluated, and our results suggest that the incorporation of PS in metalla-assemblies is not only an elegant method to increase solubility in biological media for TPyP but also appears to be an efficient hybrid system to treat RA by PDT.

Introduction

Achieving a high concentration of photosensitizer (PS) in target tissues remains a challenge in photodynamic therapy (PDT). When the concentration of PS in the cells is high, the absorption of energy is increased and consequently the possibility of transferring this energy to O_2 to generate radical oxygen species (ROS) is enhanced.[1–3] However, most synthetic photoactive compounds are poorly soluble in biological media, and to circumvent this drawback, they are often coupled to carriers. Among stratagems to transport PS, the most common is to encapsulate or bind the PS to nanoparticles.[4–6] The use of nanoparticles not only increases the physiological solubility of the PS but also, in the case of tumors, favours its accumulation through the enhanced permeability and retention (EPR) effect.[6,7] Alternative systems reported to deliver PSs use dendritic micelles.[8] Micelles not only help to transport PSs, but also largely prevent degradation before reaching their target.[9] Low-density lipoproteins (LDLs) associated to PSs is another of the many promising delivery systems.[10] LDLs have a high propensity to accumulate preferably within tumors whereby the concentration of PS in these cells can be amplified, thus enhancing the PDT effect.

In recent years, our group has demonstrated the great potential of ruthenium-based assemblies to transport PSs and other drugs to cells.[11,12] These physiologically soluble structures have an internal cavity in which a compound of the appropriate size and lipophilicity can be hosted. In addition, the toxicity is generally low (μM range) and the stability in biological media high. Once inside cells, the PS guest can be released from the cage and activated, thus giving rise to ROS. The effectiveness *in vitro* has already been demonstrated in cancer cells.[12,13] Herein, a different approach is used, which instead of transporting the PS inside the metallacage as a guest, the PS itself is part of the metallacage structure (Fig. 1).[14] Therefore, we eliminate the need of releasing the PS from the cage once inside the cells,[15] as the PS is available for irradiation at all times.

[a]*Institut de Chimie, Université de Neuchâtel, Avenue de Bellevaux 51, CH-2000 Neuchâtel, Switzerland. E-mail: bruno.therrien@unine.ch*
[b]*Université de Limoges, Laboratoire PEIRENE UR 22722, Faculté de Pharmacie, F-87025 Limoges, France. E-mail: bertrand.liagre@unilim.fr*
[c]*Service d'Orthopédie-Traumatologie, CHRU Dupuytren, 2 avenue Martin Luther King, 87042 Limoges Cedex, France*
[d]*Service de Rhumatologie, CHRU Dupuytren 2, 16 rue Bernard Descottes, 87042 Limoges Cedex, France*

†Electronic supplementary information (ESI) available: UV-vis and fluorescence spectra of **C1**, **C2**, **Zn-C1**, **Zn-C2** and **Co-C2**. See DOI: **https://doi.org/10.1039/d2dt00917j**

‡These authors contributed equally to the work.

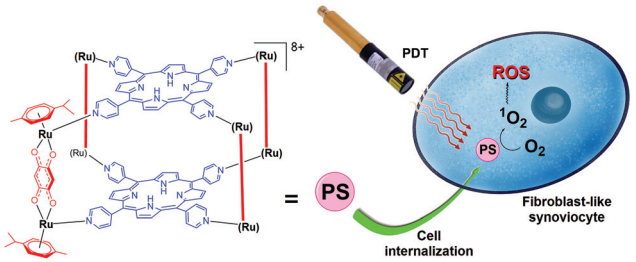

Fig. 1 Cellular uptake of physiologically soluble ruthenium metallacages containing TPyP (blue) in its structure, and subsequent PDT and production of ROS after internalization.

Compounds derived from porphyrins have already been tested in PDT to treat rheumatoid arthritis (RA) with different outcomes.[16–21] The structure of porphyrins is based on a tetrapyrrole ring. It is a rigid structure with conjugated double bonds that allows efficient delocalization of electrons. This favours the excitation of the system by irradiation and energy transmission to another molecule, explaining its extensive use in PDT. We have used TPyP as a PS because it can be coordinated directly to dinuclear arene ruthenium(II) complexes, such as $[Ru_2(\eta^6\text{-}p\text{-}^iPrC_6H_4Me)_2Cl_2(\mu\text{-}C_6H_2O_4\text{-}\kappa O)]$ and $[Ru_2(\eta^6\text{-}p\text{-}^iPrC_6H_4Me)_2Cl_2(\mu\text{-}C_2O_4\text{-}\kappa O)]$, *via* Ru–$N_{Py}$ bond, to give rise to cubic cages (C). We also believe that the presence of two TPyP panels per metallacages can reduce the dose necessary for PDT activity.[22–24] Therefore, to verify the effectiveness of our arene ruthenium tetrapyridylporphyrin-based assemblies, we have tested five compounds with different structural features including three TPyP derivatives and two dinuclear arene ruthenium clips (Fig. 2). The benzoquinonato and oxalato dinuclear arene ruthenium clips modulate the distance between the two panels of the cube, thus modifying the structure and potentially the electronic property of the assembly. The influence of metals in the center of the tetrapyrrole ring, diamagnetic (Zn^{2+}) and paramagnetic (Co^{2+}), was also studied. In addition, we have carried out photocytotoxicity and inflammatory activity evaluations in fibroblast-like synoviocytes (FLS) from patients with RA. The purpose of PDT in RA is to reduce

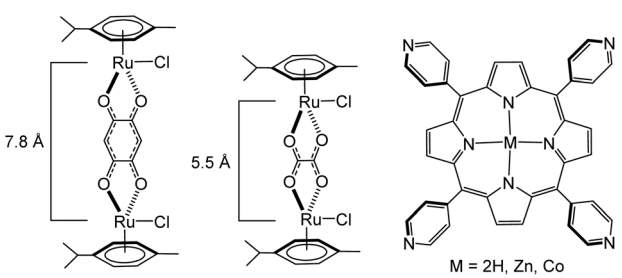

Fig. 2 The benzoquinonato and oxalato dinuclear arene ruthenium clips with the distances between the metallic atoms, as well as the structures of the TPyP porphyrin derivatives: 5,10,15,20-tetra(pyridyl-4-yl)-21*H*,23*H*-porphine (2H–TPyP), Zn(II)-5,10,15,20-tetra(pyridyl-4-yl)porphine (Zn–TPyP) and Co(II)-5,10,15,20-tetra(pyridyl-4-yl)porphine (Co–TPyP).

persistent synovitis, despite targeted biological and synthetic disease modifying anti-rheumatic drugs, and to avoid surgery.[25,26]

Materials and methods

Synthesis of compounds

Porphyrin 2H–TPyP was purchased from Sigma-Aldrich, while Zn–TPyP and Co–TPyP were obtained from Porphychem (Dijon, France), and all compounds were used as received. The metallacages $[Ru_8(\eta^6\text{-}p\text{-}^iPrC_6H_4Me)_8(\mu^4\text{-}2H\text{-}TPyP\text{-}\kappa N)_2(\mu\text{-}C_6H_2O_4\text{-}\kappa O)_4][CF_3SO_3]_8$ (**C1**), $[Ru_8(\eta^6\text{-}p\text{-}^iPrC_6H_4Me)_8(\mu^4\text{-}Zn\text{-}TPyP\text{-}\kappa N)_2(\mu\text{-}C_6H_2O_4\text{-}\kappa O)_4][CF_3SO_3]_8$ (**Zn-C1**), $[Ru_8(\eta^6\text{-}p\text{-}^iPrC_6H_4Me)_8(\mu^4\text{-}2H\text{-}TPyP\text{-}\kappa N)_2(\mu\text{-}C_2O_4\text{-}\kappa O)_4][CF_3SO_3]_8$ (**C2**), $[Ru_8(\eta^6\text{-}p\text{-}^iPrC_6H_4Me)_8(\mu^4\text{-}Zn\text{-}TPyP\text{-}\kappa N)_2(\mu\text{-}C_2O_4\text{-}\kappa O)_4][CF_3SO_3]_8$ (**Zn-C2**) and $[Ru_8(\eta^6\text{-}p\text{-}^iPrC_6H_4Me)_8(\mu^4\text{-}Co\text{-}TPyP\text{-}\kappa N)_2(\mu\text{-}C_2O_4\text{-}\kappa O)_4][CF_3\ SO_3]_8$ (**Co-C2**), were synthesized as reported in the literature.[27,28]

The fluorescence quantum yields of the metallacages were determined using standard instruments. Fluorescence spectra (Fig. S6–S10†) were performed in dimethyl sulfoxide (DMSO) on a FLS980 spectrometer from Edinburgh Instruments (550–800 nm), using 5,10,15,20-tetraphenylporphin dissolved in toluene as an internal reference. UV-vis spectra were carried out on a SI Analytics model UvLine 9400 (Xenon lamp) spectrophotometer (Fig. S1–S5†), in 1.5 mL polystyrene cuvettes (wavelength range 280–800 nm). Both, fluorescence and UV-vis spectra were carried out by dilution of compounds (10 nM) in DMSO, which was bought from Acros Organics and used as received.

Preparation of human synovial cells

RA synoviocytes were isolated from fresh synovial biopsies obtained from four RA patients undergoing finger arthroplasty. All patients fulfilled the 1987 American Rheumatism Association criteria for RA.[29] The mean age of the patients was 67.4 ± 3.2 years (range 53–81 years). The mean disease duration was 8.7 ± 2.3 years. At the time of surgery, the disease activity score (DAS 28) was greater than 3.2. These activities were approved by local institutional review boards, and all subjects gave written informed consent. Synovia were minced and digested with 1.5 mg mL^{-1} collagenase–dispase for 3–4 h at 37 °C as previously described.[30] After centrifugation, cells were resuspended in DMEM supplemented with 10% FCS, 4.5 g L^{-1} D-glucose, 25 mM Hepes, 100 U mL^{-1} penicillin, and 100 μg mL^{-1} streptomycin (Gibco BRL) in a humidified atmosphere containing 5% (v/v) CO_2 at 37 °C. After 48 h, nonadherent cells were removed. Adherent cells (macrophage-like and FLS) were cultured in complete medium, and at confluence, cells were trypsinized and only the FLS were passed. These cells were used between passages 4 and 8, when they morphologically resembled FLS after an indirect immunofluorescence study (see Culture of human RA FLS). RA FLS were cultured 45–60 days before experimentation. This delay allowed the elimination of all possible interactions resulting from any preoperative treatment (with nonsteroidal anti-inflammatory drugs,

analgesics, disease-modifying antirheumatic drugs, or steroids).

Culture of human RA FLS and treatment

Between passages 4 and 8, RA FLS were trypsinized. Cell count and survival rate were determined, and cells were plated in culture plates or flasks (Falcon, Oxnard, CA, USA). Survival rate, measured by trypan blue dye exclusion[31] at the start and the end of culture, was always greater than 95%. FLS (10^5) from RA patients were used for an indirect immunofluorescence study.[32] The following monoclonal antibodies were used: 5B5 (anti-prolyl hydroxylase) for fibroblasts at a 1/50 dilution (Dako, Burlingame, CA, USA), JC/70A (anti-CD31), for endothelial cells at 1/50 (Dako), and RMO52 (anti-CD14) for macrophages at 1/50 (Immunotech). The negative control was a mouse antibody of the same isotype (Immunotech). Incubations were performed at room temperature for 30 min. Binding of monoclonal antibodies was visualized using fluorescein (DTAF)-conjugated goat anti-mouse antibody (Immunotech) at a 1/50 dilution.

Antiproliferative assays

The *in vitro* evaluation was carried out under aseptic conditions. 3-(4,5-Dimethylthiazol-2-yl)-2,5-diphenyltetrazolium bromide (MTT) and L-glutamine were purchased from Sigma-Aldrich. RA FLS cells were collected in fresh DMEM culture medium by trypsinization. Approximately 700 000 cells were poured in 10 ml of medium and softly homogenized. 100 µl of this solution were added per well in a 96-well plate (7000 cells per well) and the cells were incubated for 24 h at 37 °C in the presence of 5% CO_2. Then, 100 µL of the PS solution in increasing concentration were dispensed per row in the plate and incubated 24 h in the same conditions. The compounds were dissolved in DMSO (1 mM) just before use and then added in the culture medium in the desired concentrations. The concentration of DMSO in the cell medium was never exceeding 0.025%. After incubation, the medium was changed carefully with 100 µL of complete medium (without red phenol). Subsequently, irradiation was performed using a red-light source, CureLight®, PhotoCure ASA at 630 nm for 30 min (dose 72 J cm^{-2}). After the irradiation, the 96-well plate was incubated 18 h. After that, 10 µl of a MTT solution (5 g l^{-1}) was added and the 96-well plate was put again inside the incubator for 4 h. Then, the media was removed and 200 µl of DMSO added in each well, followed by stirring the plate softly for 3 min. Absorbance after the MTT assay was carried out at 540 nm by a Dynex Triad Multi Mode Microplate Reader (Dynex Technologies). The assays were executed in triplicate. Cytotoxicity evaluation in the dark was carried out by repeating the same protocol without irradiation.

Protein extraction and western-blot analysis

For total protein extraction, RA FLS were washed in PBS, and the total cell pool was centrifuged at 200*g* for 5 min at 4 °C and homogenized in RIPA lysis buffer (50 mM HEPES, pH 7.5, 150 mM NaCl, 1% sodium deoxycholate, 1% NP-40, 0.1% SDS, and 20 mg mL^{-1} of aprotinin) containing protease inhibitors (Complete™ Mini, Roche Di-agnostics) according to the manufacturer's instructions. Proteins (60 µg) were separated by electrophoresis on 10% SDS–PAGE gels and transferred to polyvinylidene fluoride (PVDF) membranes (Amersham Pharmacia Biotech, Saclay, France), which were then probed with a cyclooxygenase-2 (COX-2) human primary antibody (Cayman Chemical, Bertin Pharma, Montigny le Bretonneux, France). After incubation with a secondary antibody (Dako France S.A. S., Trappes, France), blots were developed using the ECL Plus Western Blotting Detection System (Amersham Pharmacia Biotech) and G: BOX system (Syngene, Ozyme, Saint Quentin en Yvelines, France). Membranes were then reblotted with human anti-β-actin (Sigma-Aldrich, Saint Quentin Fallavier, France) used as a loading control.

Assay of COX-2 activity and IL-1β production

RA FLS were maintained in DMEM supplemented with 10% (v/v) FCS, 4.5 g l^{-1} D-glucose, 100 U mL^{-1} penicillin and 100 µg mL^{-1} streptomycin. The cells were grown in a humidified incubator at 37 °C in the presence of 5% CO_2. The 2×10^6 RA FLS cells were seeded in a 25 cm^2 flask and incubated during 24 h. Then, the volume of the PS solution to reach the IC_{50} values was added, and the cells incubated for 24 h. The medium was removed and replaced by medium without red phenol, like previously. Then, cells were irradiated at 630 nm for 30 min (dose 72 J cm^{-2}) and incubated 18 h. The non-irradiated cells were kept in the incubator the same time. After this, LPS (1 µg ml^{-1}) was added to the medium of irradiated and non-irradiated cells, and the cells were incubated for an additional 4 h. Cells were trypsinized and culture medium supernatant isolated. The prostaglandin E_2 (PGE_2)[33] and interleukin-1β (IL-1β)[34] levels were quantified in culture media supernatants from treated and control cells by enzyme immunoassay using an ELISA Kit (Cayman Chemical and Thermo Fisher Scientific, respectively). The results were expressed by the average of three independent experiments.

Statistical analysis

All quantitative results were expressed as the mean ± 3 standard deviations (SEM) of separate experiments using Excel (Microsoft Office, Version 2019). Statistical significance was evaluated by the two-tailed unpaired Student's *t*-test, *P*-value <0.001 (***).

Results and discussion

Structural features of ruthenium-based assemblies

The metallacages (**C**), which are soluble in physiological media, are synthesized by reacting dinuclear arene ruthenium complexes with tetrapyridylporphyrins (TPyP). Introduction of different building blocks (clips and panels) in the metallacages (Fig. 3) allows an evaluation of the influence of these modifications on the PDT effect. First, these cubic cages present three different PS (2H–TPyP, Zn–TPyP and Co–TPyP) separated

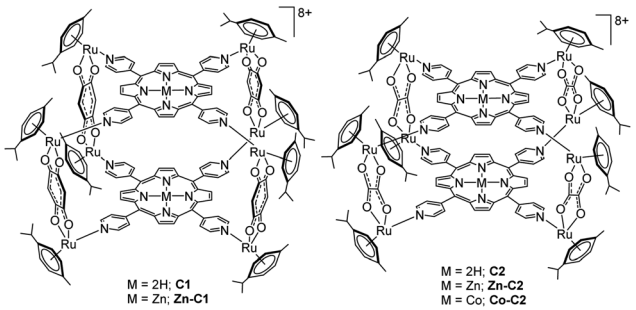

Fig. 3 Arene ruthenium metallacages used in this work. All octa-cationic assemblies were isolated as their triflate salts.

by a distance that is determined by the size of the dinuclear arene ruthenium clip (Fig. 2). Therefore, by changing the size of the ruthenium clip, we can modulate the PS separation, and determine how the distance between the two PS influences their PDT efficiency. It is known that other tetrapyrroles can give rise to aggregation phenomena, which reduces the production of singlet oxygen and then limits the production of ROS.[35,36] This is because tetrapyrroles like porphyrin show strong π–π coupling, thanks to their planar structure. However, it was demonstrated how similar cubic metalla-assemblies with TPyP efficiently inhibit the intramolecular stacking of porphyrin blocks.[37] Furthermore, these compounds are positively charged (8+), and electronic repulsion between these cationic assemblies should prevent the formation of large aggregates. These two characteristics might have a positive impact on the PDT effect.

In addition, we have used a zinc (Zn–TPyP) and a cobalt-based tetrapyridylporphyrin panel (Co–TPyP) to prepare analogous assemblies (**Zn-C1**, **Zn-C2** and **Co-C2**). The influence of the diamagnetic and paramagnetic metals on the PS can therefore be evaluated. It has been reported that diamagnetic metals such as Zn^{2+} can favour fluorescence and consequently reduce ROS production, worsening the efficacy of PDT.[38] Furthermore, paramagnetic metals such as Co^{2+} quench fluorescence due to electron transfer between the excited compound and the metal cation,[39] and therefore, no PDT effect should be observed for the **Co-C2** derivative. Therefore, introduction of metals within the TPyP panels can indicate if the photoactivity of the PS is modified or not when being part of a metalla-assembly.

Photocytotoxicity of metallacages

The results of the photocytotoxicity are presented in Table 1. The influence of the different structural parameters is evident and they alter the PDT effect. First of all, it is worth highlighting the excellent result obtained with **C1**, achieving the lowest IC_{50} (8 nM) (Fig. 4). To the best of our knowledge, no compound reported in the literature has showed such a low IC_{50} in PDT for RA *in vitro*. In addition, the phototoxic index (PI), the IC_{50} ratio between non-irradiated and irradiated cells, is greater than 125 (Table 1), which makes **C1** a PDT agent with high potential. In addition, the IC_{50} of **Zn-C1**, **C2** and **Zn-C2**

Table 1 Results of the MTT assays. Irradiation after 24 h of incubation with PS, λ = 630 nm, 72 J cm^{-2} for 30 min. IC_{50} values were calculated fitting the curve to a second-degree polynomial ± 3 sigma deviations. The maximum concentration tested was 1 μM. Quantum yields (ϕ_F) were calculated using TPP as an internal standard at 25 °C. Phototoxic index (PI) is the ratio between living cells in the dark and after irradiation

PS	IC_{50} (nM) light	IC_{50} (nM) dark	ϕ_F (%)	PI
C1	8 ± 3	>1000	0.9	>125
Zn-C1	91 ± 7	>1000	2.7	>11
C2	22 ± 7	>1000	1.7	>46
Zn-C2	185 ± 8	>1000	2.8	>5
Co-C2	>1000	>1000	0	n.d.[a]

[a] Not determined (n.d.).

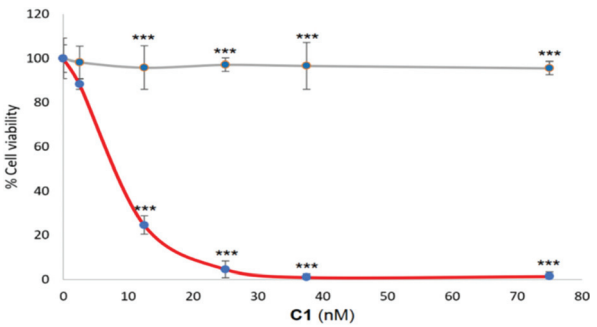

Fig. 4 MTT assays of **C1** in the dark (grey line) and after irradiation (630 nm, 72 J cm^{-2}, 30 min) (red line) in RA FLS. Statistical significance determined by the two-tailed unpaired Student's *t*-test, *p*-value <0.001 (***).

are also excellent, although they are outshined by the great performance shown by **C1**. On the other hand, **Co-C2** did not show any photocytotoxic activity, as expected for Co(II) porphyrin derivative.[39] Regarding the Zn(II) derivatives, higher fluorescence is observed (see ESI†), which translates into a lower production of ROS.[38] Both **C1** and **C2** have a higher phototoxicity than their Zn analogues (**Zn-C1** and **Zn-C2**), the IC_{50} concentrations being more than eleven times lower for **C1** and more than eight times lower for **C2** when compared to **Zn-C1** and **Zn-C2**, respectively. It is worth noting that **C1** shows a lower fluorescence quantum yield (ϕ_F) than **C2** and the Zn-derivatives (Table 1), confirming that high ϕ_F does not necessarily translate into high phototoxicity.

The main difference between **C1** and **C2** is the distance that separate the two porphyrin units in the metallacages. The results suggest that when the distance is shorter, the PDT efficiency is reduced. The IC_{50} of **C1** and **Zn-C1**, which are built from 2,5-dioxydo-1,4-benzoquinonato spacers, are less than half the IC_{50} values of the smaller oxalato analogues, **C2** and **Zn-C2** respectively. This can be rationalized by an intramolecular energy transfer phenomena between the two porphyrin panels, thus resulting in quenching. As reported in the literature, quenching and energy transfer phenomena between photo-active molecules can appear without collision or direct contact, this phenomenon is known as Resonance Energy

Transfer (RET).[40] This energy transfer is expressed by an equation formulated by Förster, which is directly related to the distance between the photo-active molecules, and it is susceptible to small changes.[41] It is established that when two PS are at short distance from each other the possibility of quenching increases significantly. The distance between the two TPyP panels is not static, since the structure can be distorted in solution.[27,28,42] However, an approximate distance can be determined from the dinuclear arene ruthenium metallaclips (Fig. 2). In **C2** and **Zn-C2**, the distance between the ruthenium atoms is linked to the oxalato ligand, and it is ≈5.5 Å.[42] On the other hand, in **C1** and **Zn-C1** the distance is dictated by the benzoquinonato ligand, and it is ≈7.8 Å.[43] Therefore, a greater distance suggests minimal quenching, which leads to better PDT efficiency, in agreement with the results obtained. Finally, it should be noted that none of the tested compounds showed cytotoxicity in the dark at 1 μM concentration (Table 1), which is an essential characteristic for a good PS. Fig. 5 shows the comparison in RA FLS treated with **C2** (22 nM), showing cellular damage in the irradiated RA FLS and no apparent changes in the non-irradiated cells.

Inflammatory study

As previously reported, PDT with porphyrin derivatives as well as other PS is susceptible to lead to overexpression of COX-2 and production of PGE_2, which could translate into inflammation in the treated tissue after therapy.[33] RA FLS give rise to cytokines such as tumor necrosis factors (TNF) and interleukins (IL), which increase COX-2 production, an enzyme that catalyzes the formation of PGE_2 from arachidonic acid.[44,45] PGE_2 is a vasodilator that can lead to inflammation.[46] To combat this unwanted effect, it is possible to use COX-2 inhibitors such as NS-398.[33] With this in mind, we decided to evaluate the inflammatory activity of our compounds after PDT, analyzing the expression of COX-2 in the treated cells and the production of PGE_2 and the presence of IL-1β in the culture media. On the other hand, since the cobalt compound did not show cytotoxic activity in the MTT assays, we decided not to include this compound in the anti-inflammatory evaluation, focusing on the four most promising ruthenium-based assemblies (**C1**, **C2**, **Zn-C1** and **Zn-C2**).

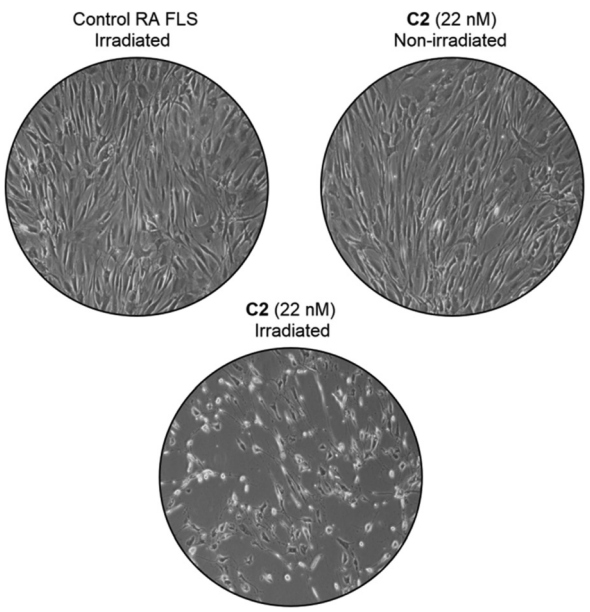

Fig. 5 Effect of PDT on RA FLS using **C2** at 22 nM concentration (IC_{50}) after 24 h. Control cells 24 h after irradiation (top left), cells with **C2** but not irradiated (top right), and cells with **C2** and irradiation (down) (red-light 630 nm, 72 J cm^{-2} for 30 min).

COX-2 expression

As seen in Fig. 6, these porphyrin-based compounds induce COX-2 overexpression after PDT. However, **C1** shows surprising results, since the expression of COX-2 is not very different from the control experiments. Indeed, the overexpression of COX-2 was greater in the irradiated samples than in the non-irradiated ones. It should be noted that the expression of COX-2 is directly related to the results observed in the photocytotoxic evaluation. When a lower concentration is used, that is, when the IC_{50} is lower, the overexpression of COX-2 is also lower. This suggests that by reducing the dose of the drug, one could reduce inflammatory adverse effects, while maintaining a good photoactivity.

PGE_2 production and IL-1β level

Given the overexpression of COX-2, we can expect overproduction of PGE_2 (see Table 2). This overproduction can lead to inflammation after PDT, although as discussed above, it can be reduced or eliminated by the presence of COX-2 inhibitors. Again, it is worth noting the result of **C1**, whose production of PGE_2 is significantly close to that observed in the control sample. In addition, the same observation is made with the IC_{50}, although it is expected since PGE_2 is directly related to COX-2, as already mentioned.[44,45] This again points to the fact that a lower dose of the drug might generate fewer adverse effects in PDT.

IL-1β is a pro-inflammatory cytokine and it has been reported as one of the cytokines responsible for COX-2 expression.[47] Surprisingly, IL-1β does not appear to be directly related to the overexpression of COX-2 and overproduction of

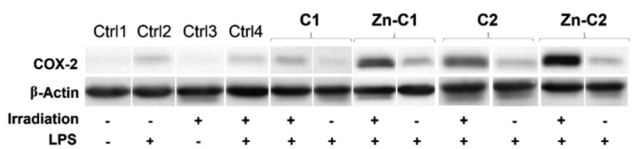

Fig. 6 Evaluation of COX-2 expression after PDT. Cells (2×10^6) were cultured in DMEM (FBS 10%, L-glutamine 1%, penicillin 100 U mL^{-1}, streptomycin 100 μg mL^{-1}) during 24 h and treated with the corresponding PS. After 24 h, the medium was replaced by DMEM without red phenol and irradiated at 630 nm (72 J cm^{-2}, 30 min). After 18 h, LPS (1 μg mL^{-1}) was added in the medium to stimulate the expression of COX-2 during 4 h. Finally, trypsinization and isolation of cells was performed. COX-2 expression was determined by western-blot using β-actin as a protein loading control. All experiments were done in triplicate. Non-irradiated cells were treated as irradiated. Control samples were treated as treated cells (see Antiproliferative assays).

Table 2 PGE_2 and IL-1β production. The assays were performed in triplicate using the protocol provided by the ELISA kit. The data were treated as explained in this protocol. The cells were treated by PDT with each compounds as described in the experimental section. The control sample was treated exactly like others, that is, 18 h after the irradiation dose, 1 μg mL^{-1} of LPS was added to the medium and the cells were incubated for 4 h, then trypsinized and the cells and supernatant were isolated. The results are expressed by the average of three independent experiments. The results are expressed by the average of triplicate assays ± 3 standard deviation (SEM)

PS	PGE_2 (pg ml^{-1})	IL-1β (pg ml^{-1})
Ctrl	286.6 ± 0.1	1.8 ± 0.7
C1	352.2 ± 21.0	2.1 ± 0.7
Zn-C1	444.4 ± 7.4	1.8 ± 1.4
C2	390.0 ± 11.8	2.0 ± 1.2
Zn-C2	457.1 ± 1.9	1.6 ± 0.4
Co-C2	n.d.[a]	n.d.

[a] Not determined (n.d.).

PGE_2 (Table 2). The results obtained are closed to those of the control sample. This suggests that, in our case, other cytokines are involved in this overexpression, which has also been reported in other studies.[48]

Conclusions

Among the five metallacages, **C1** shows the best potential as a PDT agent to treat RA synovitis, having an excellent phototoxicity (IC_{50} = 8 nM) and a low general toxicity (IC_{50} > 1000 nM). Moreover, as suggested by the results obtained in the inflammatory evaluation, the adverse effects associated with PDT should be significantly reduced with our compounds. Indeed, when using **C1**, COX-2 expression and PGE_2 production are lower and close to control samples, thus potentially limiting post-therapy joint inflammation. We have also observed that IL-1β does not appear to be involved in the inflammation effects, indicating that other cytokines may be involved in the expression of COX-2. Overall, these results invite us to continue investigating the use of such metallacages in PDT, not only in RA, but also in other pathologies such as cancer.

Author contributions

Conceptualization, M. G.-V., B. T. and B. L.; Methodology, M. G.-V., L. P. and J.-L. C.; Validation, D. Y. L., B. T. and B. L.; Writing—original draft preparation, M. G.-V. and P. V.-S.; Writing—review and editing, B. T. and B. L. All authors have read and agreed to the published version of the manuscript.

Informed consent statement

Informed consent was obtained from all subjects involved in the study. Written informed consent was obtained from the patients for research purposes.

Conflicts of interest

The authors declare no conflict of interest.

Acknowledgements

We thank all of the people involved in the project POLYTHEA, and especially Stéphanie Leroy-Lhez, Johann Bouclé, and Nidia Maldonado-Carmona for access to fluorescence equipment and for valuable discussions. Also, Aline Pinon and Dima Youssef Diab for all their help and advice during the *in vitro* evaluation.

This research was funded by the European Union's Horizon 2020 research and innovation programme under the Marie Skłodoska-Curie grant agreement no. 764837.

References

1 I. J. Macdonald and T. J. Dougherty, Basic principles of photodynamic therapy, *J. Porphyrins Phthalocyanines*, 2001, **5**, 105–129.
2 Á. Juarranz, P. Jaén, F. Sanz-Rodríguez, J. Cuevas and S. González, Photodynamic therapy of cancer. Basic principles and applications, *Clin. Transl. Oncol.*, 2008, **10**, 148–154.
3 J. Kennedy, R. H. Pottier and D. C. Pross, Photodynamic therapy with endogenous protoporphyrin: IX: basic principles and present clinical experience, *J. Photochem. Photobiol., B*, 1990, **6**, 143–148.
4 I. Roy, T. Y. Ohulchanskyy, H. E. Pudavar, E. J. Bergey, A. R. Oseroff, J. Morgan, T. J. Dougherty and P. N. Prasad, Ceramic-based nanoparticles entrapping water-insoluble photosensitizing anticancer drugs: A novel drug– carrier system for photodynamic therapy, *J. Am. Chem. Soc.*, 2003, **125**, 7860–7865.
5 S. Bouramtane, L. Bretin, A. Pinon, D. Leger, B. Liagre, L. Richard, F. Brégier, V. Sol and V. Chaleix, Porphyrin-xylan-coated silica nanoparticles for anticancer photodynamic therapy, *Carbohydr. Polym.*, 2019, **213**, 168–175.
6 L. Bretin, A. Pinon, S. Bouramtane, C. Ouk, L. Richard, M. L. Perrin, A. Chaunavel, C. Carrion, F. Brégier, V. Sol, V. Chaleix, D. Y. Leger and B. Liagre, Photodynamic therapy activity of new porphyrin-xylan-coated silica nanoparticles in human colorectal cancer, *Cancers*, 2019, **11**, 1474.
7 H. Maeda, The enhanced permeability and retention (EPR) effect in tumor vasculature: the key role of tumor-selective macromolecular drug targeting, *Adv. Enzyme Regul.*, 2001, **41**, 189–207.
8 N. Nishiyama, Y. Morimoto, W. D. Jang and K. Kataoka, Design and development of dendrimer photosensitizer-incorporated polymeric micelles for enhanced photodynamic therapy, *Adv. Drug Delivery Rev.*, 2009, **61**, 327–338.

9 C. F. van Nostrum, Polymeric micelles to deliver photosensitizers for photodynamic therapy, *Adv. Drug Delivery Rev.*, 2004, **56**, 9–16.

10 E. Reddi, Role of delivery vehicles for photosensitizers in the photodynamic therapy of tumours, *J. Photochem. Photobiol., B*, 1997, **37**, 189–195.

11 B. Therrien, Transporting and Shielding Photosensitisers by Using Water–Soluble Organometallic Cages: A New Strategy in Drug Delivery and Photodynamic Therapy, *Chem. – Eur. J.*, 2013, **19**, 8378–8386.

12 F. Schmitt, J. Freudenreich, N. P. Barry, L. Juillerat-Jeanneret, G. Süss-Fink and B. Therrien, Organometallic cages as vehicles for intracellular release of photosensitizers, *J. Am. Chem. Soc.*, 2012, **134**, 754–757.

13 G. Gupta, E. Denoyelle-Di-Muro, J. P. Mbakidi, S. Leroy-Lhez, V. Sol and B. Therrien, Delivery of porphin to cancer cells by organometallic Rh(III) and Ir(III) metalla-cages, *J. Organomet. Chem.*, 2015, **787**, 44–50.

14 N. P. E. Barry, O. Zava, P. J. Dyson and B. Therrien, Synthesis, Characterization and Anticancer Activity of Porphyrin–Containing Organometallic Cubes, *Aust. J. Chem.*, 2010, **63**, 1529–1537.

15 N. P. E. Barry, O. Zava, P. J. Dyson and B. Therrien, Excellent Correlation between Drug Release and Portal Size in Metalla-Cage Drug-Delivery Systems, *Chem. – Eur. J.*, 2011, **17**, 9669–9677.

16 B. A. Allison, P. H. Pritchard, A. M. Richter and J. G. Levy, The plasma distribution of benzoporphyrin derivative and the effects of plasma lipoproteins on its biodistribution, *Photochem. Photobiol.*, 1990, **52**, 501–507.

17 K. B. Trauner, R. Gandour-Edwards, M. Bamberg, S. Shortkroff, C. Sledge and T. Hasan, Photodynamic Synovectomy Using Benzoporphyrin Derivative in an Antigen-induced Arthritis Model for Rheumatoid Arthritis, *Photochem. Photobiol.*, 1998, **67**, 133–139.

18 K. Trauner, R. Gandour-Edwards, M. Bamberg, N. S. Nishioka, T. Flotte, S. Autry and T. Hasan, Influence of light delivery on photodynamic synovectomy in an antigen-induced arthritis model for rheumatoid arthritis, *Lasers Surg. Med.*, 1998, **22**, 147–156.

19 E. Torikai, Y. Kageyama, E. Kohno, T. Hirano, Y. Koide, S. Terakawa and A. Nagano, Photodynamic therapy using talaporfin sodium for synovial membrane from rheumatoid arthritis patients and collagen-induced arthritis rats, *Clin. Rheumatol.*, 2008, **27**, 751–761.

20 A. Hansch, O. Frey, M. Gajda, G. Susanna, J. Boettcher, R. Bräuer and W. A. Kaiser, Photodynamic treatment as a novel approach in the therapy of arthritic joints, *Lasers Surg. Med.*, 2008, **40**, 265–272.

21 F. Schmitt, L. Lagopoulos, P. Käuper, N. Rossi, N. Busso, J. Barge, G. Wagnières, C. Laue, C. Wandrey and L. Juillerat-Jeanneret, Chitosan-based nanogels for selective delivery of photosensitizers to macrophages and improved retention in and therapy of articular joints, *J. Controlled Release*, 2010, **144**, 242–250.

22 S. I. Moriwaki, J. Misawa, Y. Yoshinari, I. Yamada, M. Takigawa and Y. Tokura, Analysis of photosensitivity in Japanese cancer–bearing patients receiving photodynamic therapy with porfimer sodium (PhotofrinTM), *Photodermatol., Photoimmunol. Photomed.*, 2001, **17**, 241–243.

23 J. Usuda, H. Kato, T. Okunaka, K. Furukawa, H. Tsutsui, K. Yamada, Y. Suga, H. Honda, Y. Nagatsuka, T. Ohira, M. Tsuboi and T. Hirano, Photodynamic therapy (PDT) for lung cancers, *J. Thorac. Oncol.*, 2006, **1**, 489–493.

24 T. J. Dougherty and S. L. Marcus, Photodynamic therapy, *Eur. J. Cancer*, 1992, **28**, 1734–1742.

25 M. H. Buch, Defining refractory rheumatoid arthritis, *Ann. Rheum. Dis.*, 2018, **77**, 966–969.

26 G. Nagy, N. M. T. Roodenrijs, P. M. J. Welsing, *et al.*, EULAR definition of difficult-to-treat rheumatoid arthritis, *Ann. Rheum. Dis.*, 2021, **80**, 31–35.

27 N. P. Barry, M. Austeri, J. Lacour and B. Therrien, Highly efficient NMR enantiodiscrimination of chiral octanuclear metalla-boxes in polar solvent, *Organometallics*, 2009, **28**, 4894–4897.

28 A. N. Oldacre, M. R. Crawley, A. E. Friedman and T. R. Cook, Tuning the Activity of Heterogeneous Cofacial Cobalt Porphyrins for Oxygen Reduction Electrocatalysis through Self–Assembly, *Chem. – Eur. J.*, 2018, **24**, 10984–10987.

29 F. C. Arnett, S. M. Edworthy, D. A. Bloch, D. J. Mcshane, J. F. Fries, N. S. Cooper, L. A. Healey, S. R. Kaplan, M. H. Liang, H. S. Luthra, T. A. Medsger, D. M. Mitchell, D. H. Neustadt, R. S. Pinals, J. G. Schaller, J. T. Sharp, R. L. Wilder and G. G. Hunder, The American Rheumatism Association 1987 revised criteria for the classification of rheumatoid arthritis, *Arthritis Rheumatol.*, 1988, **31**, 315–324.

30 B. Liagre, P. Vergne-Salle, C. Corbiere, J. L. Charissoux and J. L. Beneytout, Diosgenin, a plant steroid, induces apoptosis in human rheumatoid arthritis synoviocytes with cyclooxygenase-2 overexpression, *Arthritis Res. Ther.*, 2004, **6**, 1–11.

31 T. T. Glant, J. J. Jacobs, G. Molnár, A. S. Shanbhag, M. Valyon and J. O. Galante, Bone resorption activity of particulate–stimulated macrophages, *J. Bone Miner. Res.*, 1993, **8**, 1071–1079.

32 C. Bonnet, P. Bertin, J. Cook-Moreau, H. Chable-Rabinovitch, R. Treves and M. Rigaud, Lipoxygenase products and expression of 5-lipoxygenase and 5-lipoxygenase-activating protein in human cultured synovial cells, *Prostaglandins*, 1995, **50**, 127–135.

33 C. Fidanzi-Dugas, B. Liagre, G. Chemin, A. Perraud, C. Carrion, C. Y. Couquet, R. Granet, V. Sol and D. Y. Léger, Analysis of the in vitro and in vivo effects of photodynamic therapy on prostate cancer by using new photosensitizers, protoporphyrin IX-polyamine derivatives, *Biochim. Biophys. Acta, Gen. Subj.*, 2017, **1861**, 1676–1690.

34 M. Gallardo-Villagrán, L. Paulus, J.-L. Charissoux, S. Sutour, P. Vergne-Salle, D. Y. Leger, B. Liagre and

B. Therrien, Evaluation of Ruthenium-Based Assemblies as Carriers of Photosensitizers to Treat Rheumatoid Arthritis by Photodynamic Therapy, *Pharmaceutics*, 2021, **13**, 2104.

35 C. Jing, R. Wang, H. Ou, A. Li, Y. An, S. Guo and L. Shi, Axial modification inhibited H-aggregation of phthalocyanines in polymeric micelles for enhanced PDT efficacy, *Chem. Commun.*, 2018, **54**, 3985–3988.

36 S. Tuncel, F. Dumoulin, J. Gailer, M. Sooriyaarachchi, D. Atilla, M. Durmuş, D. Bouchu, H. W. Savoie, W. R. Boyle and V. Ahsen, A set of highly water-soluble tetraethyleneglycol-substituted Zn(II) phthalocyanines: synthesis, photochemical and photophysical properties, interaction with plasma proteins and in vitro phototoxicity, *Dalton Trans.*, 2011, **40**, 4067–4079.

37 X. Jiang, Z. Zhou, H. Yang, C. Shan, H. Yu, L. Wojtas, M. Zhang, Z. Mao, M. Ming Wang and P. J. Stang, Self-assembly of porphyrin-containing metalla-assemblies and cancer photodynamic therapy, *Inorg. Chem.*, 2020, **59**, 7380–7388.

38 A. Kamkaew, S. H. Lim, H. B. Lee, L. V. Kiew, L. Y. Chung and K. Burgess, BODIPY dyes in photodynamic therapy, *Chem. Soc. Rev.*, 2013, **42**, 77–88.

39 V. V. Volchkov, V. L. Ivanov and B. M. Uzhinov, Induced intersystem crossing at the fluorescence quenching of laser dye 7-amino-1,3-naphthalenedisulfonic acid by paramagnetic metal ions, *J. Fluoresc.*, 2010, **20**, 299–303.

40 K. K. Ng and G. Zheng, Molecular interactions in organic nanoparticles for phototheranostic applications, *Chem. Rev.*, 2015, **115**, 11012–11042.

41 H. Hevekerl, T. Spielmann, A. Chmyrov and J. Widengren, Forster resonance energy transfer beyond 10 nm: exploiting the triplet state kinetics of organic fluorophores, *J. Phys. Chem. B*, 2011, **115**, 13360–13370.

42 Y. F. Han, Y. J. Lin, L. H. Weng, H. Berke and G. X. Jin, Stepwise formation of "organometallic boxes" with half-sandwich Ir, Rh and Ru fragments, *Chem. Commun.*, 2008, **3**, 350–352.

43 N. P. Barry and B. Therrien, Host-guest chemistry in the hexanuclear (arene)ruthenium metalla-prismatic cage $[Ru_6(p\text{-cymene})_6(tpt)_2(dhnq)_3]^{6+}$, *Eur. J. Inorg. Chem.*, 2009, 4695–4700.

44 W. H. S. Nasry, J. C. Rodriguez-Lecompte and C. K. Martin, Role of COX-2/PGE2 mediated inflammation in oral squamous cell carcinoma, *Cancers*, 2018, **10**, 348.

45 M. S. Sung, E. G. Lee, H. S. Jeon, H. J. Chae, S. J. Park, Y. C. Lee and W. H. Yoo, Quercetin inhibits IL-1β-induced proliferation and production of MMPs, COX-2, and PGE_2 by rheumatoid synovial fibroblast, *Inflammation*, 2012, **35**, 1585–1594.

46 G. P. Downey, R. S. Gumbay, D. E. Doherty, J. F. LaBrecque, J. E. Henson, P. M. Henson and G. S. Worthen, Enhancement of pulmonary inflammation by PGE_2: evidence for a vasodilator effect, *J. Appl. Physiol.*, 1988, **64**, 728–741.

47 R. Newton, L. M. Kuitert, M. Bergmann, I. M. Adcock and P. J. Barnes, Evidence for involvement of NF-κB in the transcriptional control of COX-2 gene expression by IL-1β, *Biochem. Biophys. Res. Commun.*, 1997, **237**, 28–32.

48 K. Shimomura, T. Kanamoto, K. Kita, Y. Akamine, N. Nakamura, T. Mae, H. Yoshikawa and K. Nakata, Cyclic compressive loading on 3D tissue of human synovial fibroblasts upregulates prostaglandin E2 via COX-2 production without IL-1β and TNF-α, *Bone Jt. Res.*, 2014, **3**, 280–288.

